Integrity of the yeast mitochondrial genome, but not its distribution and inheritance, relies on mitochondrial fission and fusion

Christof Osman[a,b], Thomas R. Noriega[a,b], Voytek Okreglak[a,b], Jennifer C. Fung[c], and Peter Walter[a,b,1]

[a]Howard Hughes Medical Institute, [b]Department of Biochemistry and Biophysics, and [c]Department of Obstetrics, Gynecology and Reproductive Sciences, University of California, San Francisco, CA 94158-2517

Contributed by Peter Walter, January 26, 2015 (sent for review January 9, 2015; reviewed by Thomas D. Fox and Nikolaus Pfanner)

Mitochondrial DNA (mtDNA) is essential for mitochondrial and cellular function. In *Saccharomyces cerevisiae*, mtDNA is organized in nucleoprotein structures termed nucleoids, which are distributed throughout the mitochondrial network and are faithfully inherited during the cell cycle. How the cell distributes and inherits mtDNA is incompletely understood although an involvement of mitochondrial fission and fusion has been suggested. We developed a LacO-LacI system to noninvasively image mtDNA dynamics in living cells. Using this system, we found that nucleoids are nonrandomly spaced within the mitochondrial network and observed the spatiotemporal events involved in mtDNA inheritance. Surprisingly, cells deficient in mitochondrial fusion and fission distributed and inherited mtDNA normally, pointing to alternative pathways involved in these processes. We identified such a mechanism, where we observed fission-independent, but F-actin–dependent, tip generation that was linked to the positioning of mtDNA to the newly generated tip. Although mitochondrial fusion and fission were dispensable for mtDNA distribution and inheritance, we show through a combination of genetics and next-generation sequencing that their absence leads to an accumulation of mitochondrial genomes harboring deleterious structural variations that cluster at the origins of mtDNA replication, thus revealing crucial roles for mitochondrial fusion and fission in maintaining the integrity of the mitochondrial genome.

mtDNA | Dnm1 | Fzo1 | mitochondria | yeast

Mitochondrial DNA (mtDNA) is essential for respiratory growth of all eukaryotic cells, and all multicellular organisms depend on mtDNA for their development. Not surprisingly, given the fundamental importance of mtDNA, mutations within mtDNA have been identified as the cause for a plethora of human diseases (1). mtDNA in *Saccharomyces cerevisiae* encodes for seven essential subunits of the respiratory chain, one protein and two RNA subunits of the mitochondrial ribosome, 24 tRNAs, and the RNA subunit of RNase P (2). Every cell contains 50–100 copies of mtDNA that are organized into nucleoprotein complexes termed nucleoids, each containing 1–10 copies of mtDNA (3, 4). Nucleoids are distributed throughout the mitochondrial network, which is likely important for equivalently supplying spatially separated mitochondrial segments with mitochondrially encoded proteins.

How the distribution of mtDNA throughout the mitochondrial network is established and maintained is not fully understood. Previous work from our laboratory and others has shown that the movement of nucleoids within the mitochondrial network is limited, suggesting that the mechanisms of nucleoid distribution are tightly interlinked with the dynamics of mitochondria themselves (5, 6). Mitochondria undergo constant fusion and fission events that are mediated by dedicated machineries, with the central components Fzo1 and Dnm1 required for fusion and fission, respectively (7). Recently, we have provided support for a role of mitochondrial fission in mtDNA distribution. We have shown that mtDNA localizes to sites of Dnm1-dependent mitochondrial fission and that it is segregated after scission to both of the newly generated mitochondrial tips (8). Localizing mtDNA to the newly formed tips would then allow transport of mitochondrial tips and mtDNA to distal parts in the cell, where fusion with the mitochondrial network may drive mtDNA distribution. Such a mechanism would be particularly important during inheritance of mtDNA to daughter buds during cell division, where mtDNA needs to be transported over a relatively large distance. In *S. cerevisiae*, mitochondria are inherited in a myosin- and F-actin–dependent process, in which a mitochondrial tubule invades the budding daughter cell and is subsequently anchored at the distal membrane (9). An active mtDNA partition and inheritance apparatus has been postulated (6); however, the spatiotemporal relationship between the inheritance of mitochondria and the inheritance of mtDNA has not been examined.

If mitochondrial fusion and fission were essential for the distribution and inheritance of mtDNA, their loss would impair the process. Indeed, fusion-defective cells lose mtDNA (10, 11), most likely due to excessive fragmentation. By contrast, however, fission-defective cells, as well as cells defective in fusion and fission, remain capable of respiratory growth, indicating that a functional mitochondrial genome must be maintained (10, 12). These observations suggest that fission-independent mechanisms must exist that facilitate mtDNA inheritance.

In this work, we investigated the role of mitochondrial fusion and fission in mtDNA distribution and inheritance. Through the development of a noninvasive method to quantify the spatial

Significance

Mitochondrial DNA (mtDNA) encodes essential subunits of respiratory complexes, which are responsible for the generation of ATP through oxidative phosphorylation in mitochondria. Copies of mtDNA are distributed throughout the mitochondrial network and are faithfully inherited during the cell cycle. We have developed a novel tool in *Saccharomyces cerevisiae* that allows us to watch mtDNA dynamics in living cells and to characterize its distribution and inheritance. We show that, surprisingly, mitochondrial fusion and fission are dispensable for both processes. The absence of fusion and fission events, however, leads to the accumulation of rearranged and dysfunctional mitochondrial genomes. These results reveal crucial roles of mitochondrial fusion and fission in maintaining the quality and integrity of the mitochondrial genome.

Author contributions: C.O. and P.W. designed research; C.O. performed research; C.O., T.R.N., and J.C.F. contributed new reagents/analytic tools; C.O., T.R.N., V.O., and P.W. analyzed data; and C.O., V.O., and P.W. wrote the paper.

Reviewers: T.D.F., Cornell University; and N.P., University of Freiburg.

The authors declare no conflict of interest.

Freely available online through the PNAS open access option.

[1]To whom correspondence should be addressed. Email: peter@walterlab.ucsf.edu.

This article contains supporting information online at www.pnas.org/lookup/suppl/doi:10.1073/pnas.1501737112/-/DCSupplemental.

organization of mtDNA within mitochondrial tubules, we found that cells deficient in fusion and fission maintain a WT distribution of mtDNA. Live-cell imaging showed that this distribution is facilitated by the de novo generation of tubules from the sides of existing tubules, a process coupled to the spatial positioning of mtDNA to the newly formed tip. Unexpectedly, although dispensable for maintaining mtDNA distribution and inheritance, fusion and fission were required to maintain the integrity of the mitochondrial genome.

Results

A Novel Approach to Noninvasively Label mtDNA in Live Cells. Visualization of mtDNA and its dynamics in living yeast cells so far have depended on the use of intercalating dyes or the use of mtDNA-interacting proteins that have been tagged with fluorescent proteins. However, mtDNA is highly susceptible to intercalating dyes, which interfere with mtDNA metabolism and drive mtDNA loss (13). In agreement with this view, we observed that the use of the DNA-intercalating fluorescent dye 4',6-diamidino-2-phenylindole (DAPI), at concentrations used for labeling mtDNA, induced the rapid formation of petite cells that have lost functional copies of mtDNA (Fig. 1 *A* and *B*) and led to abnormal cell morphologies, demonstrating DAPI's acute toxicity (Fig. 1*C*). Similarly, tagging mtDNA-binding proteins with fluorescent proteins may interfere with their function, which in turn may alter mtDNA-related processes. Furthermore, it has been shown in yeast that the mtDNA-interacting protein Mgm101 forms foci even in cells completely lacking mtDNA (14), raising the possibility that not all foci revealed by mtDNA-binding proteins may accurately report on the presence of mtDNA. To overcome these methodological shortcomings, we developed a novel system to study mtDNA dynamics in living cells. To this end, we adapted, for mtDNA, the LacO-LacI-GFP system that has been established for studying bacterial DNA and eukaryotic nuclear DNA dynamics (15, 16). We first introduced an array of ~40 identical LacO repeats upstream of the *COX2* gene into mtDNA by biolistic transformation (*Materials and Methods*) and expressed a LacI-GFP protein fused to the Su9 mitochondrial targeting sequence. This approach proved unsuccessful because the repeats were rapidly eliminated due to their sequence identity and the high DNA recombination activity in yeast mitochondria. To overcome these problems, we generated a synthetic array consisting of 11 LacO repeats, each containing different combinations of mutations that do not interfere with binding of the LacI protein (17). We further reduced the degree of homology within the array by separating the LacO repeats with spacers of varying length and sequence. To improve the fluorescent signal at these shorter arrays, we expressed a triple GFP-tagged mitochondrially targeted LacI protein (mt-3xGFP-LacI) (Fig. 1*D*).

Expression of mt-3xGFP-LacI in WT cells devoid of mt-LacO repeats led to a uniform distribution throughout the mitochondrial network whereas expression of mt-3xGFP-LacI in cells harboring the mt-LacO repeats led to clearly discernible foci that distributed throughout the mitochondrial network (Fig. 1*E*). We noted that the fluorescent intensity of the 3xGFP LacI signal varied for different foci in the same cell (Fig. 1 *E* and *F*), which is in line with previous work that suggested that nucleoids contain a varying number of copies of the mitochondrial genome (18). To test whether the observed foci accurately represented nucleoids, we costained the cells with DAPI and observed near perfect

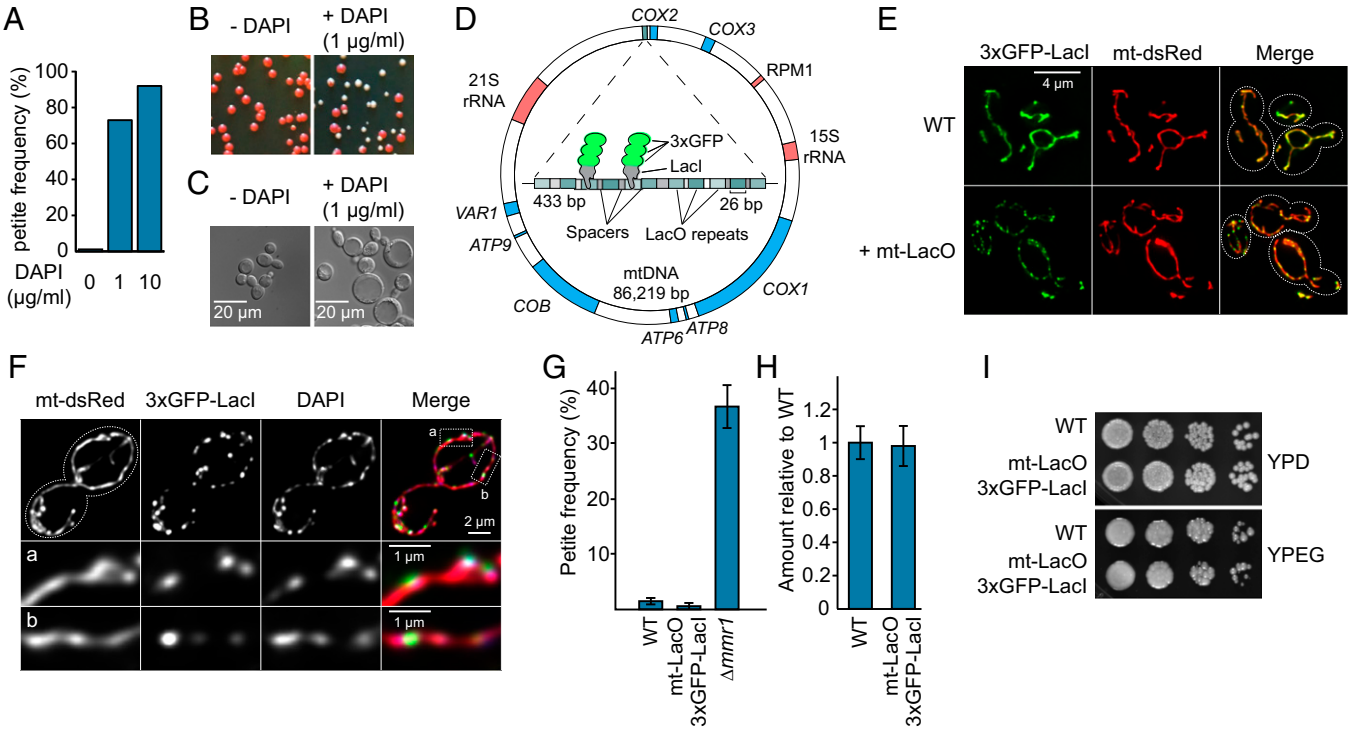

Fig. 1. The mt-LacO-LacI system. (*A*) Histogram showing the petite frequency of cells grown for 6 h in the absence or presence of indicated amounts of DAPI in the growth medium. (*B*) Representative image of the petite frequency assay. White colonies indicate respiratory deficiency. (*C*) Cells grown overnight in the presence of DAPI (1μg/mL) were examined by light microscopy. (*D*) Schematic representation of the mt-LacO-LacI system. The length of individual genetic elements is drawn to scale. (*E*) Maximum intensity Z-projections of WT cells or cells harboring the mt-LacO repeats, each expressing mt-3xGFP-LacI and mt-dsRed. (*F*) Maximum intensity Z-projection of an mt-LacO-LacI cell treated with DAPI (1 μg/mL). Close-ups of mitochondrial segments are shown that illustrate colocalization of the mt-3xGFP-LacI and the DAPI signal. (*G*) The petite frequency was determined for WT, mt-LacO-LacI, and Δ*mmr1* cells. (*H*) qPCR analysis of total levels of mtDNA relative to nuclear DNA in WT and mt-LacO-LacI cells. (*I*) Serial dilutions of WT and mt-LacO-LacI cells were spotted on YPD or YPEG plates containing a fermentable or nonfermentable carbon source, respectively.

colocalization of DAPI-positive signals within mitochondria and mt-3xGFP-LacI foci, validating the mt-LacO-LacI system as a faithful system to visualize mtDNA (Fig. 1*F*). Interestingly, at many foci the 3xGFP-LacI signal was observed as a much more spatially confined signal, resembling diffraction-limited spots, compared with the DAPI signal. The likely reason for this observation is that DAPI staining reveals the entire spread of mtDNA whereas the mt-LacO-LacI system reports on the precise locus containing the integrated LacO repeats. A more spatially confined 3xGFP-LacI signal compared with the DAPI signal was also observed for relatively bright foci that likely contain multiple copies of mtDNA (Fig. 1 *F*, *b*). These data indicate that the LacO arrays of these multiple copies are spatially constrained at such nucleoids, perhaps by higher organization in which homologous sequences are juxtaposed.

To test whether the mt-LacO-LacI system interfered with mtDNA maintenance, we assayed cells harboring the mt-LacO repeats and expressing the 3xGFP-LacI protein (henceforth referred to as "mt-LacO-LacI cells") for the occurrence of petite cells. The mt-LacO-LacI cells displayed no increase in the frequency of petite formation relative to WT cells. In contrast, cells lacking Mmr1, which is involved in mitochondrial inheritance, showed a clear increase in petite frequency in this assay (Fig. 1*G*). We also examined the effects of the mt-LacO-LacI system on overall levels of mtDNA by quantitative PCR analysis and found identical mtDNA amounts compared with WT cells (Fig. 1*H*). Additionally, growth of cells harboring the mt-LacO-LacI system on fermentable or nonfermentable carbon sources was indistinguishable from WT cells (Fig. 1*I*). Taken together, these data show that the mt-LacO-LacI system is a faithful and minimally invasive way to study mtDNA dynamics in living cells.

WT Cells Maintain an Equivalent Distance Between Nucleoids. To quantitatively define the distribution of mtDNA within mitochondria, we imaged mt-LacO-LacI cells expressing mitochondrially targeted dsRed (mt-dsRed). We converted the images into 3D coordinates by skeletonizing the mitochondrial network, such that it was represented as a branched line running through the network, and by assigning coordinates to the center of each detected GFP-LacI spot (Fig. 2*A* and Movie S1).

We first quantified the relationship between the length of the mitochondrial network and the number of nucleoids in each cell. Strikingly, when the nucleoid number was plotted against the network length of mitochondria for every analyzed cell, we observed a strong correlation between both, revealing a link between the length of the mitochondrial network and the number of nucleoids contained in it (Fig. 2*B*). We further distinguished between the mother cell and the bud in our analysis and found that, irrespective of the stage of the bud development, the relationship was maintained. The correlation was also evident in very small buds, where only short mitochondrial segments had entered the bud.

Next, we quantified the distribution of mtDNA within the mitochondrial network. Using the 3D coordinate dataset, we projected the centroid coordinate of each nucleoid onto the closest point of the skeletonized mitochondrial filaments. We then determined the distance of every nucleoid along the filament to all its neighboring nucleoids (Fig. 2*A*, *Right*). This analysis was done for 840 nucleoids in the mitochondrial networks of 23 cells. A histogram of the data shows a distinct distribution of internucleoid distances around a most frequently observed distance of ~800 nm (Fig. 2*C*). We then tested whether this distribution was different from a randomly generated distribution. To eliminate any possible effects of the overall mitochondrial network shape on the random distribution of nucleoids, we used the identical mitochondrial networks found in each cell and randomly distributed the same number of nucleoids within them. The internucleoid distance in the random dataset was clearly distinct from the real dataset, with the majority of distances falling into the closest distance bin (Fig. 2*C*, *Bottom*). Comparison of the real and the random datasets revealed a statistically significant difference ($P < 0.001$) (*Materials and Methods*). Thus, these analyses unequivocally show that the distribution of nucleoids within the mitochondrial network is nonrandom, with closely spaced nucleoids observed less frequently than expected by a random distribution.

mtDNA Is Spatially Associated with Mitochondrial Tips. In agreement with our previous observation that mtDNA localizes to sites of mitochondrial fission and that it is segregated to the mitochondrial tips produced after scission (8), we noted that mtDNA was closely associated with mitochondrial tips. We quantitatively assessed this phenomenon by measuring the distance from every mitochondrial tip to the next nucleoid. The analysis revealed a strong enrichment of mtDNA close to mitochondrial tips. In 69% of the cases, mtDNA was detected closer than 500 nm to the tip of a mitochondrial tubule (Fig. 2*D*). Analysis of the same parameter for the simulated random distribution of mtDNA showed only 33% of tips associated with mtDNA closer than 500 nm (Fig. 2*D*, *Bottom*).

Transport of mtDNA in Mitochondrial Tips. We previously hypothesized that localization of mtDNA to tips may be important to transport mtDNA over large distances, where movement of mtDNA through mitochondrial tubules may be inefficient (8). Tip localization of mtDNA would be particularly important during the cell cycle, where long-distance transport is essential for the inheritance of mitochondria and mtDNA into budding daughter cells. To test this notion, we examined live mt-LacO-LacI cells to assess whether mtDNA remained associated with tips during inheritance. Strikingly, in 90% of the cases ($n = 40$), mtDNA associated with the leading tip of a mitochondrial tubule that invaded the daughter bud. Time-lapse microscopy revealed a dynamic association of mtDNA with the leading mitochondrial tip throughout the inheritance event (Fig. 2*E* and Movie S2), which suggests that the mtDNA–tip association facilitates faithful mtDNA inheritance.

mtDNA Distribution Is Unaltered in Cells with Defective Mitochondrial Fusion and Fission. The above data, together with our previous observations of mtDNA segregating to mitochondrial tips during mitochondrial fission, support the hypothesis that fission-mediated tip localization of mtDNA may be an important determinant for its distribution and inheritance. To test whether fission deficiency results in compromised mtDNA distribution and inheritance, we imaged mt-LacO-LacI cells lacking the fission component Dnm1 (Δ*dnm1*). However, Δ*dnm1* cells grown in dextrose media formed a tight network of interconnected mitochondrial tubules making it impossible to unambiguously skeletonize the mitochondrial network and to accurately quantify the distribution of mtDNA. To overcome this limitation, we imaged mtDNA in mt-LacO-LacI cells lacking both the mitochondrial fusion and the fission machinery (Δ*dnm1*Δ*fzo1*). Fluorescence microscopy analysis of these mt-LacO-LacI cells expressing mt-dsRed showed that, in accordance with previously published data, Δ*dnm1*Δ*fzo1* cells displayed a reticulated and tubular mitochondrial network (12), which was on average slightly shorter than the network of WT cells (WT, 27.1 ± 4.4 μm vs. Δ*dnm1*Δ*fzo1*, 21.9 ± 4.4 μm) (Table S1). Surprisingly, Δ*dnm1*Δ*fzo1* cells contained distinct, spatially separated mtDNA foci (Fig. 3*A* and Movie S3), and quantitative analysis of the distribution of 635 nucleoids within the mitochondrial networks from 23 cells revealed that, as in WT cells, the mitochondrial nucleoid number scales with mitochondrial length (Fig. 3*B*). Remarkably, analysis of the internucleoid distance showed the same distance distribution as WT cells centered around 800 nm (Fig. 3*C*) and was significantly different from a simulated random

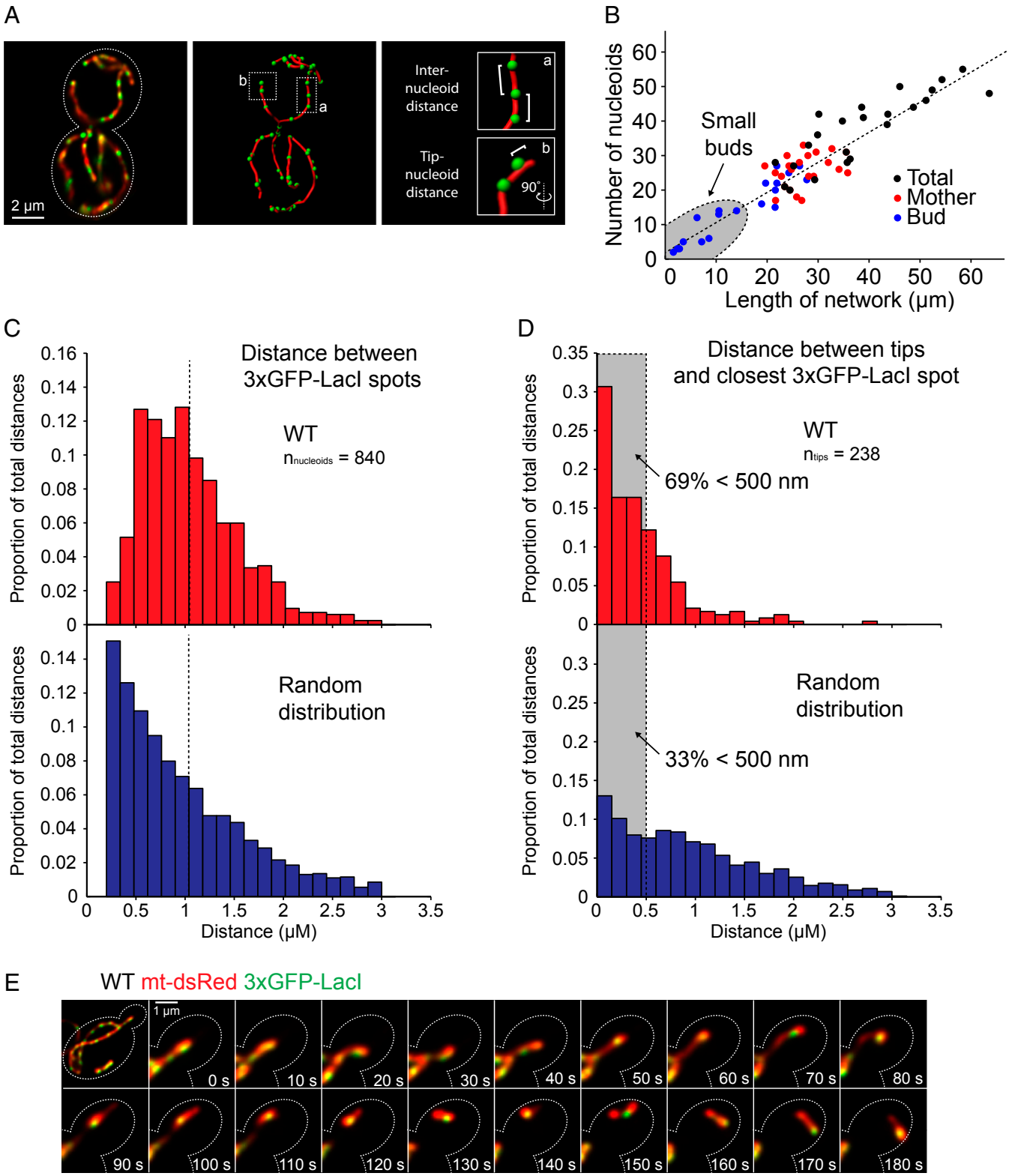

Fig. 2. mtDNA distribution in WT cells. (*A*) Maximum intensity Z-projection of a representative WT mt-LacO-LacI cell expressing mt-dsRed (*Left*). Image of the same cell with skeletonized mitochondria and spheres at positions of mtDNA (*Middle*). Illustration of the distance measurements between nucleoids or between mitochondrial tips and nucleoids (*Right*) (*Bottom Right* image is rotated by 90°; compare Movie S1). (*B*) The number of nucleoids is plotted against the network length of the mitochondria. Datasets from mother, daughter, or both cells are distinguished; the data for small buds are indicated. (*C*) Distances between each nucleoid and the closest neighboring nucleoids along the mitochondrial filament (see *A*) of experimentally determined or randomly distributed nucleoids were determined for 23 cells, binned and plotted in a histogram. The dashed line indicates the mean distance between nucleoids. Note that the mean distances are similar for the real and the simulated dataset. The *x* axis was limited to 3.5 µm; less frequently observed longer distances are thus omitted from the figure. (*D*) Distances between mitochondrial tips and the closest nucleoid (see *A*) were determined for the real and the simulated dataset, binned, and plotted in a histogram. Distances smaller than 500 nm are highlighted. (*E*) Time-lapse microscopy of a representative WT mt-LacO-LacI cell expressing mt-dsRed shows the spatiotemporal relationship of mitochondrial and mtDNA inheritance.

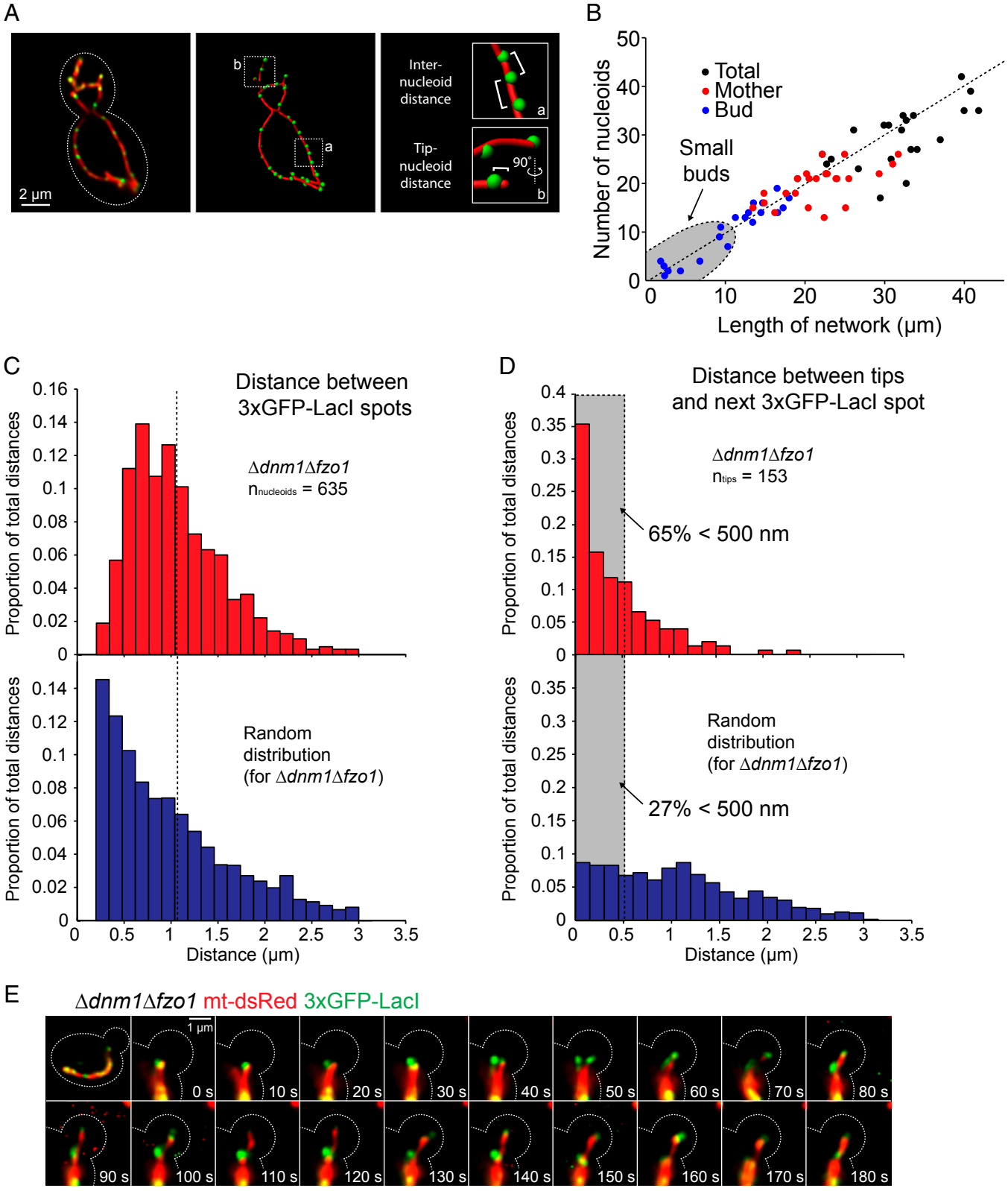

Fig. 3. mtDNA distribution in Δ*dnm1*Δ*fzo1* cells. (*A*) Maximum intensity Z-projection of a representative Δ*dnm1*Δ*fzo1* mt-LacO-LacI cell expressing mt-dsRed is shown (*Left*). Image of the same cell with skeletonized mitochondria and spheres at positions of mtDNA (*Middle*). Illustration of the distance measurements between nucleoids or between mitochondrial tips and nucleoids (*Right*) (*Bottom Right* image is rotated by 90°; compare Movie S3). (*B*) Correlation between nucleoid number and network length. (*C*) Distribution of internucleoid distances. (*D*) Distribution of nucleoid-mitochondrial-tip distances. (*E*) Time-lapse microscopy of a representative WT mt-LacO-LacI cell expressing mt-dsRed shows the spatiotemporal relationship of mitochondrial and mtDNA inheritance.

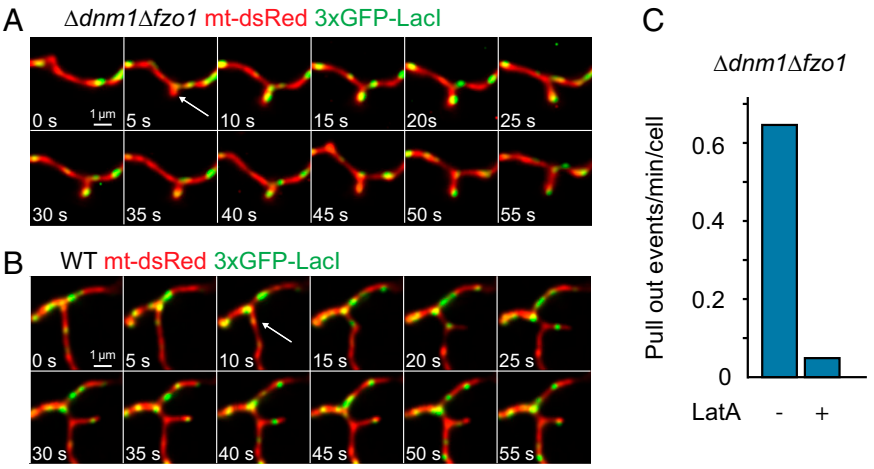

Fig. 4. Fission-independent mitochondrial tip generation. (*A* and *B*) Single frames from time-lapse microscopy of (*A*) Δ*dnm1*Δ*fzo1* or (*B*) WT cells harboring the mt-LacO-LacI system and expressing mt-dsRed. Arrows indicate the start of fission-independent tubule generation. (*C*) Δ*dnm1*Δ*fzo1* cells expressing mt-dsRed were treated with LatA or not, and Z-stacks of complete cells were acquired every 4 s for a total of 160 s, and fission-independent generation of mitochondrial tips was quantified in 40 cells in each sample (compare Movie S5 with Movie S6).

distribution generated for identical mitochondrial networks (Fig. 3*C*, *Bottom*).

We were surprised to find that, despite the absence of mitochondrial fission, Δ*dnm1*Δ*fzo1* cells contained only a slightly reduced number of mitochondrial tips per cell compared with WT cells (WT, 6.6 ± 3.1 vs. Δ*dnm1*Δ*fzo1*, 4.1 ± 1.9) (Table S1). These tips, similarly to WT cells, were closely associated with mtDNA, which was significantly different from the simulated random distribution of mtDNA in these networks (Fig. 3*D*).

We next used live-cell microscopy to test whether the mtDNA containing mitochondrial tips in Δ*dnm1*Δ*fzo1* cells were used during long-range transport of mtDNA. As observed for WT cells, mitochondrial tips invaded the bud and mtDNA remained associated to the tip throughout this process. In agreement with the absence of mitochondrial fission in these cells, we did not observe any release of mitochondrial fragments into the bud, as observed for WT cells (Fig. 3*E* and Movie S4).

Mitochondrial Dynamics in the Absence of Mitochondrial Fusion and Fission. The presence of mitochondrial tips associated with mtDNA in Δ*dnm1*Δ*fzo1* cells was unexpected because these cells were deficient in mitochondrial fission, the only process known to generate them. To investigate whether fission-independent mechanisms exist that generate mitochondrial tips containing mtDNA, we analyzed mitochondrial and mtDNA dynamics in Δ*dnm1*Δ*fzo1* cells. As expected, no mitochondrial fission and fusion events were observed in these cells. The data, however, revealed de novo generation of mitochondrial tips that were laterally pulled or pushed out of existing tubules (Fig. 4*A*). Strikingly, the majority of de novo generated tips were closely associated with mtDNA.

We next asked whether this alternative mode of tip generation was unique to fission- and fusion-defective cells by examining identically obtained time series of WT cells. As observed for fusion- and fission-deficient cells, fission-independent tip generation was evident in the mitochondrial network in WT cells (Fig. 4*B*). Quantification of the dynamic positioning of mtDNA in mitochondrial tips of WT cells showed that, in 87% of de novo tubule generation events, mtDNA was positioned near the mitochondrial tip within the first 20 s ($n = 60$).

The mechanism underlying this form of tip generation has not been examined before. Because mitochondria are transported along the actin cytoskeleton in *S. cerevisiae*, we hypothesized that fission-independent tip generation may likewise be actin-dependent. To examine this notion, we imaged mitochondrial dynamics in cells treated with latrunculin A (LatA) that sequesters actin monomers and leads to the disassembly of the actin cytoskeleton. LatA treatment leads to Dnm1-dependent fragmentation of the mitochondrial network in WT cells, thus complicating our analysis (19). We therefore performed these experiments in Δ*dnm1*Δ*fzo1* cells. LatA treatment led to effective disassembly of the actin cytoskeleton, which was confirmed by phalloidin staining (Fig. S1). Although fission-independent tip generation was frequently observed in the absence of LatA (Fig. 4*C* and Movie S5), a drastic decrease in the frequency of these events was observed in cells after treatment with LatA (Fig. 4*C* and Movie S6). These data show that a fission-independent but actin-dependent mechanism exists for the generation of mitochondrial tips loaded with mtDNA.

Fusion and Fission Are Required for Maintaining the Integrity of the Mitochondrial Genome. The finding that fusion- and fission-deficient cells are capable of normal distribution and inheritance of mtDNA was surprising in the light of our previous observations that mtDNA is localized to the vast majority of mitochondrial fission sites (8). We considered the possibility that mitochondrial fusion and fission might be important for a function other than the distribution and inheritance of mtDNA. It has been previously hypothesized that mitochondrial fission is essential for counteracting the accumulation of dysfunctional mitochondrial genomes (20). To test this idea, we assayed WT and Δ*dnm1*Δ*fzo1* cells for the occurrence of respiration-deficient ρ^- cells that contained nonfunctional mitochondrial genomes by comparing the percentage of petite and ρ^0 (lacking mtDNA) cells using the petite frequency assay and DAPI staining, respectively. We found that ∼23% of Δ*dnm1*Δ*fzo1* cells were incapable of respiratory growth (<1% for WT) whereas all cells contained mtDNA (Fig. 5*A*), indicating that all of the petite cells were ρ^- rather than ρ^0. We further supported this conclusion by testing whether mtDNA present in Δ*dnm1*Δ*fzo1* petite cells was able to recombine with mtDNA of strains harboring either a small deletion in *COX3* (21) or a deletion of *COB* (22), both encoded in the mtDNA, to restore WT mtDNA molecules that allow respiratory growth. To this end, we crossed Δ*dnm1*Δ*fzo1* petite strains against the *cox3* and Δ*cob* tester strains and found that respiratory growth was restored by a cross to only the Δ*cob* strain (40%), only the cox3 mutant strain (12.5%), or both (15%) whereas respiratory growth of 32.5% of the petites was not complemented by either strain ($n = 40$). These results reveal heterogeneity among

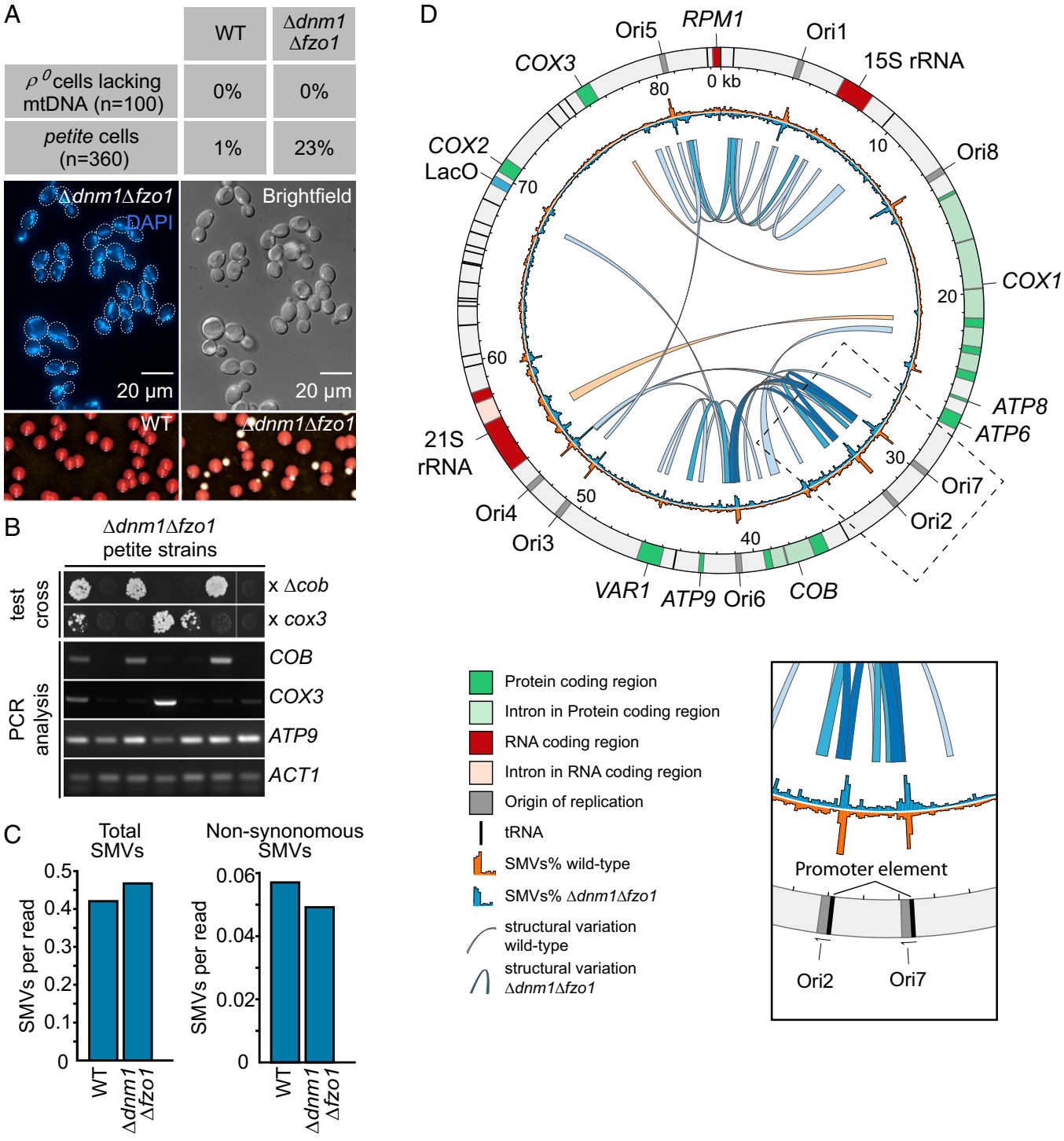

Fig. 5. Δ*dnm1Δfzo1* accumulate ρ^- genomes. (*A*, *Top*) Table reporting the ρ^0 and petite frequencies for WT and Δ*dnm1Δfzo1* cells that were determined by DAPI staining and the petite frequency assay, respectively. Representative images of DAPI-stained Δ*dnm1Δfzo1* cells with the corresponding brightfield (*Middle*) and the petite frequency assay (*Bottom*) are shown. (*B*) mtDNA complementation assay and PCR analysis of petite Δ*dnm1Δfzo1* cells. Seven individual Δ*dnm1Δfzo1* petite colonies were crossed against tester strains containing either a small deletion in the *COX3* gene or a compete deletion of the *COB* gene, and crosses were replicated onto YPEG plates. Cell growth indicates complementation of the genetic defects of mtDNA in the parental strains. Loci in the mtDNA (*COB*, *COX3*, *ATP9*) and nuclear DNA (*ACT1*) were amplified by PCR in the parental Δ*dnm1Δfzo1* petite strains used for the complementation analysis. (*C*) Analysis of small mtDNA variations (SMVs) by next-generation sequencing. Total number of SMVs (*Left*) and number of nonsynonymous SMVs detected in protein coding regions (*Right*) of WT and Δ*dnm1Δfzo1* cells. The amount of SMVs was normalized to the number of reads that aligned to the mtDNA in each sample. (*D*) The mutational landscapes of mtDNA in WT and Δ*dnm1Δfzo1* cells. The outer ring represents the mitochondrial genome, and features are indicated. The histograms in the inner rings show the percentage of detected SMV's binned into 100-bp segments for WT (blue) and Δ*dnm1Δfzo1* (orange). The arcs in the middle represent structural variations (compare Table S2) for WT (light orange) and Δ*dnm1Δfzo1* (shades of blue). Each end of the arc points to the region of mtDNA to which each of the paired reads aligned. These regions are fused in the mutant mtDNA that gave rise to the respective sequencing reads. For Δ*dnm1Δfzo1*, a darker shade of blue indicates that these variations were detected more often (compare Table S2). A region of the diagram is enlarged to illustrate SMVs and structural variations at two of the origins of replication. Promoter elements associated with the origins are indicated by a black bar.

the Δ*dnm1*Δ*fzo1* petite strains regarding genetic defects in the mtDNA (Fig. 5*B*, *Top*). We extended this analysis and probed for the presence of different loci within mtDNA in a subset of the Δ*dnm1*Δ*fzo1* petite strains by PCR analysis. Robust amplification of the *COX3* and *COB* genes from petite Δ*dnm1*Δ*fzo1* strains correlated with their ability to complement defects in the respective genes (Fig. 5*B*, *Bottom*). Furthermore, these analyses revealed that even the two petite strains of the tested subset that were unable to restore respiratory growth of either the mutant *cox3* or Δ*cob* strains contained mtDNA as *ATP9* was successfully amplified in these strains, further supporting the notion that compromised mtDNA rather than its complete loss results in respiratory insufficiency in Δ*dnm1*Δ*fzo1* petites.

Next, we aimed to characterize broadly the mutational landscape of mtDNA in WT and Δ*dnm1*Δ*fzo1* cells to identify the genetic defects that lead to respiratory-deficient progeny in Δ*dnm1*Δ*fzo1* cells containing compromised mitochondrial genomes. To this end, we extracted mtDNA from mitochondria that were isolated from cultures grown from respiratory-competent colonies of either WT or Δ*dnm1*Δ*fzo1* strains and performed paired-end next-generation sequencing. We obtained a median sequence coverage of >2,000× in each strain. First, we assessed the total number of small mtDNA variations (SMVs), including single-nucleotide variations and small deletions and insertions (<20 bp), and the number of SMVs leading to nonsynonymous changes in protein-encoding genes. In mtDNA derived from WT and Δ*dnm1*Δ*fzo1* cells, we observed comparable numbers of both types of SMVs (Fig. 5*C*). We furthermore analyzed the distribution of SMVs throughout the mtDNA and found identical distributions for both strains (Fig. 5*D*). Notably, in mtDNA from WT as well as Δ*dnm1*Δ*fzo1* cells, increased amounts of SMVs clustered at all of the eight previously identified origins of replication. In each case, these clusters coincided with a transcriptional promoter element that has been identified at all origins of replication (2). In summary, these results indicate that point mutations or small deletions and insertions are unlikely to account for the accumulation of mtDNA unable to sustain respiratory growth in Δ*dnm1*Δ*fzo1* cells. Furthermore, these analyses reveal mutational hotspots associated with the origins of replication within mtDNA.

We further analyzed our sequencing data for reads revealing structural variations in the mitochondrial genomes of WT or Δ*dnm1*Δ*fzo1* cells. For paired-end next-generation sequencing, the input DNA is fragmented into 200-bp to 1,500-bp fragments, and adapter sequences are attached to both ends. Fragments are then sequenced from both ends, which results in two reads that constitute a pair. Both reads of a pair are expected to map not farther apart than ∼1,500 bp to opposing strands on the reference genome, with the 3′ ends facing each other. We filtered our sequencing data for paired reads that violated these rules and were thus indicative of structural variations, such as deletions or inversions. We further filtered these data for variations that were detected at least twice in the dataset. In contrast to the analysis of SMVs, we detected a dramatic increase in structural variations of the mtDNA in Δ*dnm1*Δ*fzo1* cells compared with the WT (Fig. 5*D* and Table S2). We detected 35 distinct structural variations in Δ*dnm1*Δ*fzo1* cells in a total of 119 paired reads, compared with only two structural variations, each detected two times, in WT cells. Notably, the structural variations in the Δ*dnm1*Δ*fzo1* cells did not distribute evenly throughout the mitochondrial genome, but clustered in the regions between Ori5 to Ori8 and Ori4 to Ori7 (Fig. 5*D*). Remarkably, ∼62% of these rearrangements occurred within 500 bp of one of the origins of replication, regions that in aggregate span only ∼12% of the mitochondrial genome, suggesting a strong tendency for genome-wide architectural rearrangements to occur in the vicinity of the origins of replication.

In conclusion, these results reveal that fusion- and fission-deficient cells accumulate mitochondrial genomes with structural variations that lead to respiratory deficiency of their progeny.

Discussion

mtDNA inheritance, distribution, and genome integrity are critical for cell functions that require mitochondrial respiratory activity, and all of these mtDNA features have been proposed to require remodeling of the mitochondria network by fission and fusion (8, 9, 20, 23). However, experimental analysis of the effects of mitochondrial dynamics on these features of mtDNA has largely been lacking. In general, elucidation of the mechanisms that facilitate mtDNA distribution and inheritance was hampered by the lack of methods to visualize mtDNA and its dynamics in living cells. The mt-LacO-LacI system eliminates this limitation. We used this tool to systematically analyze and quantitate the spatial distribution of mtDNA within the mitochondrial network, which revealed a previously underappreciated organization. First, we found that the nucleoid number correlates with mitochondrial network length. Second, nucleoids were rather evenly spaced by ∼800 nm. Third, mtDNA was positioned near mitochondrial tips. Our data indicate that this organization is a nonrandom process, suggesting that mechanisms are in place to nonrandomly space nucleoids within the mitochondrial network. A significant technological advance provided by the mt-LacO-LacI system is the ability to follow mtDNA by live-cell time-lapse microscopy, which allowed us to determine, for the first time to our knowledge, the spatiotemporal events associated with mtDNA inheritance in *S. cerevisiae*. Our analysis suggests that the faithful localization of mtDNA to the tip of the first mitochondrial tubule invading the bud underlies the high fidelity of mtDNA inheritance.

Intriguingly, we found that fusion- and fission-deficient Δ*dnm1*Δ*fzo1* cells maintain a normal distribution of mtDNA within the mitochondrial network and faithfully inherit mtDNA during the cell cycle. In contrast, Δ*dnm1*Δ*fzo1* cells fail to maintain the integrity of the mitochondrial genome, and, as a consequence, an increased number of cells are incapable of respiratory growth. Together, these observations show that the major mtDNA-related role for mitochondrial fusion and fission in yeast cells is not to maintain its distribution and inheritance but to preserve genome integrity.

Our sequencing analysis revealed that structural variations rather than point mutations or small deletions and insertions are the nature of the accumulating nonfunctional genomes in Δ*dnm1*Δ*fzo1* cells. We further detected that the structural variations are enriched in the vicinity of the origins of replication, suggesting that initiation of replication may be prone to erroneous recombination or double-strand breaks that result in mistakes during nonhomologous end-joining. It is presently unclear how mtDNA replication is initiated in *S. cerevisiae*. Although the identification of RNA polymerase promoters at the origins of replication (2) hints toward an RNA-primed mode of replication, mtDNA can be maintained and replicated in the absence of the mitochondrial RNA polymerase, which has led to the idea that an alternative mode of replication initiation exists that involves recombination (24). Supporting such a model, recent evidence shows that recombination-driven replication is predominant in other yeast species (25, 26). Our identification of structural rearrangements of mtDNA that originate at origins of replication suggests that these origins may be sites of increased rates of recombination that could be involved in the initiation of replication in *S. cerevisiae*.

Why do such rearrangements accumulate in fusion- and fission-deficient cells, but not in WT cells? An intriguing hypothesis is that such rearrangements are generated in WT cells as well but accumulate in Δ*dnm1*Δ*fzo1* cells only because mutant genomes cannot be separated from the mitochondrial network by fission

events. Isolation of compromised copies of mtDNA into mitochondrial fragments would lead to a decline of the membrane potential in these fragments, which may act as the trigger for their destruction by mitophagy or their selective retention in the mother cell. In agreement with such a hypothesis, mathematical models suggest that mitochondrial fission and mitophagy may counteract the accumulation of mutated mitochondrial genomes (20).

We resolved the paradoxical finding that Δ*dnm1*Δ*fzo1* cells inherit mtDNA like WT cells, with mtDNA localized in the tip of a bud-invading tubule, through the identification of a fission-independent mechanism to generate mtDNA-containing mitochondrial tips. In line with previous findings that show that mitochondria are transported along the actin cytoskeleton in *S. cerevisiae* (9), de novo mitochondrial tip generation is also actin-dependent. The mechanisms that underlie tip localization of mtDNA during fission-independent tip generation are currently unknown. At least three, nonexclusive mechanisms are conceivable. First, mtDNA may be recruited and maintained at mitochondrial tip membranes by factors that bind mtDNA and preferentially bind to membranes with high curvature. Second, mtDNA movement may be restricted in specific directions by the dynamic reorganization of cristae. Third, mtDNA may be transported by a cytoskeleton-like structure internal to mitochondria, analogous to the bacterial ParM plasmid segregation machinery (27).

Taken together with our previous finding describing the segregation of mtDNA during mitochondrial fission (8), two distinct modes of mtDNA segregation exist (fission-dependent tip generation and fission-independent tube pull-out). Whether these two modes are functionally redundant or serve specialized functions remains to be determined. Regardless, tip localization of mtDNA has intriguing implications because it may provide the cell with means to "proofread" the mitochondrial genome: tips containing functional mtDNA could be preferentially chosen for distribution and/or inheritance (or alternatively for retention and/or destruction) by mechanisms that recognize local membrane potential surrounding such copies. In this regard, it is intriguing that nucleoids that are active in replication localize to sites of fission (8, 14), potentially linking the generation of new mtDNA to tip localization and subjecting them to such selection. It will be important to examine whether fission-independent tip generation is likewise associated with active mtDNA replication.

Materials and Methods

Yeast Strains and Plasmids. Yeast strains used in this study are derivatives of W303 and are listed in Table S3. Deletion of yeast genes was performed in a diploid strain as described previously (28). Diploid cells were used for all experiments, except those shown in Figs. 1*D* and 5*A*, where haploid cells were used.

For expression of the mitochondrial targeted 3xGFP-LacI protein, a construct containing 467 bp of the *CUP1* promoter, followed by the Su9 mitochondrial targeting sequence, three GFP repeats, and the LacI protein, was cloned into HO-poly-kanMX4-HO (29), which was used for single integration of P_{Cup1}-Su9-3xGFP-LacI into the HO locus. For visualization of mitochondria, cells were transformed with pvt100u-mt-dsRed.

Generation of the mt-LacO Strain. The nonrecombinable LacO array, consisting of 11 LacO repeats separated by spacers of varying length and sequence (Fig. S2), was synthesized and cloned into the EcoRI site of plasmid pPT24 (30), thus flanking the LacO repeats with regions homologous to the upstream region of the mitochondrial gene *COX2*, resulting in the plasmid pCO221. Integration of the LacO repeats into mtDNA was performed as essentially described previously (31). In brief, pCO221 was transformed into mitochondria of strain DFS160 by biolistic transformation. This strain was crossed against the strain NB40-3C harboring the *cox2-62* allele, and cells where the LacO repeats had recombined into the upstream region of *COX2* were isolated by selection on a nonfermentable carbon source. After sporulation of the resulting strain, the mtDNA harboring the LacO repeats was transferred by cytoduction into the W303 background, where mtDNA was beforehand depleted by overexpression of MGM101-GFP from an episomal plasmid (32). Successful depletion of mtDNA in the latter strain was monitored by DAPI staining. The resulting strain was crossed against a WT W303 strain of opposing mating type, in which mtDNA had been depleted by transient overexpression of MGM101-GFP.

PCR and qPCR for Determination of mtDNA Levels. Total DNA was isolated from logarithmically growing cells in imaging medium (see *Microscopy*) according to established procedures (33). Total DNA was then subjected to qPCR using the iQ-Supermix (Bio-Rad) following the manufacturer's instructions. For mtDNA and nuclear DNA, loci within the *COX3* and *ACT1* were amplified, respectively (see Table S4 for primer sequences). PCR analysis was performed with the Phusion-polymerase (see Table S4 for primer sequences). Specificity of primer pairs for mtDNA target genes was confirmed by testing them on DNA from ρ^0 cells.

Petite Frequency Assay. Haploid cells lacking the *ADE2* gene were grown in imaging medium and kept in log-phase for 24 h. Then, cells were spread on multiple YPD plates not supplemented with adenine, and white colonies were scored as petites (24).

Microscopy. For imaging, cells were grown to midlog in synthetic dextrose medium lacking tryptophan and appropriate nutrients to select for episomal plasmids and supplemented with 340 mg/L, 550 mg/L, and 430 mg/L isoleucine, leucine, and valine, respectively, to prevent parsing of nucleoids (34). Cells were immobilized in glass-bottom culture dishes (Bioptechs, Inc.) with Con A (1 mg/mL) and overlaid with 1 mL of fresh medium. Cells were imaged on an OMX microscope equipped with a 100× 1.4 N.A. objective lens (35). Z-stacks were acquired over 7 μm in 0.2-μm increments. For time-lapse movies, only 3-μm-thick Z-stacks were collected. Images for each fluorophore were acquired with different EMCCD cameras (iXON; Andor), and images were aligned postcapture using alignment parameters generated from images of 0.1-μm fluorescent microspheres (TetraSpeck; Invitrogen).

The imaging experiments examining the importance of the actin cytoskeleton for fission-independent tubule generation were performed on a Nikon Eclipse Ti equipped with a spinning disk confocal (CSU-X1; Yokogawa), EMCCD camera (iXon3 897; Andor), and a 100× 1.49 N.A. objective. Cells were resuspended in media containing 100 μM latrunculin A [2% (vol/vol) DMSO] and incubated for 15 min at room temperature before imaging. The latrunculin A concentration was maintained in the medium during imaging.

For staining of F-actin, cells were fixed by addition of paraformaldehyde [32% (wt/vol)] to a final concentration of 4% (wt/vol) to the medium. After incubation at room temperature for 10 min, cells were pelleted and resuspended in PBS containing 4% (wt/vol) paraformaldehyde and incubated for an additional 60 min. Cells were washed with PBS, and actin was stained by resuspension of cells in 10 μL of 6.6 μM Alexa Fluor 633 phalloidin (Life Technologies) in methanol.

Image Processing and Analysis. Microscopic images were deconvolved using Huygens software (Scientific Volume Imaging) and measured point-spread functions for each channel. Mitochondria were skeletonized with Imaris (Bitplane), and mtDNA foci were assigned with the spot-finding function of Imaris. Accurate skeletonization and foci assignment was manually inspected and corrected if necessary. For determination of the distances between mtDNA foci and between mtDNA foci and mitochondrial tips, the mitochondrial filament and the mtDNA coordinates were exported to MATLAB (MathWorks), and distances along the filament were determined by custom scripts.

Statistical Analysis. To assess the statistical significance of the difference between the experimental and the simulated distance distribution, the *P* value was determined empirically. For each cell, the parameter z was determined by calculating the SD of the measured distances and dividing it by the average distance. The parameter z was determined for all cells, and the average value T was determined. The same analysis was performed for 1,000 simulations, and the T values of the experimental and each simulated dataset were compared. The *P* value was calculated by dividing the number of times a smaller T value for the simulation compared with the experimental dataset was obtained by the number of simulations.

Next-Generation Sequencing and Sequence Analysis. For next-generation sequencing analysis of mtDNA, mitochondria were isolated from yeast strains (yPW1933 and yPW1934) grown in YP supplemented with 2% (wt/vol) galactose and 0.5% lactate as described previously (36), and DNA was phenol/chloroform extracted from isolated mitochondria. Sequencing-ready DNA

libraries were prepared with the NexteraXT sample preparation kit (Illumina) by following the manufacturer's instructions. Sequencing was performed on the Illumina MiSeq instrument with the MiSeq v2 500 cycle reagent kit (Illumina). The obtained reads of the WT sample were first aligned to an mtDNA reference genome (available at www.yeastgenome.org) with the SeqMan NGen (DNAStar) software, and deviations from the reference genome were manually corrected. SMVs were identified with SeqManPro (DNAStar) software after aligning the paired-end reads to the corrected reference genome using SeqMan NGen software (minMatchPercent = 80, minAlignedLength = 50, filterDeepLayout = false, and default settings for all other parameters). SMVs were quantified by counting the number of reads containing mismatches at each position of the corrected mitochondrial reference genome. Mutations with a per site frequency of >4.5% were omitted from this analysis to remove the effect of extreme mutational hotspots on the quantification of mtDNA mutations (37). Structural variations were detected with the SVDetect tool (38) after aligning the reads to the corrected reference genome with Bowtie2 using the default parameters (39). The illustration presented in Fig. 5*D* was prepared with the Circos visualization software (40).

ACKNOWLEDGMENTS. We thank the members of the P.W. and Jodi Nunnari laboratories for critical discussions on this work, John Sedat for sharing invaluable advice and insights on live-cell microscopy, Tom Fox for reagents and helpful discussions during the development of the mt-LacO-LacI system, Eric Chow from the Center of Advanced Technology at the University of California, San Francisco, for advice during next-generation sequencing experiments, and Martin Ott, Thomas Langer, and Jean diRago for providing reagents. C.O. and V.O. were supported by Human Frontier Science Program and Leukemia Lymphoma Society fellowships, respectively. T.R.N. was supported by the National Institute of General Medicine Initiative for Maximizing Student Development and National Science Foundation graduate research fellowships. P.W. is an investigator of the Howard Hughes Medical Institute.

1. Nunnari J, Suomalainen A (2012) Mitochondria: In sickness and in health. *Cell* 148(6):1145–1159.
2. Turk EM, Das V, Seibert RD, Andrulis ED (2013) The mitochondrial RNA landscape of Saccharomyces cerevisiae. *PLoS ONE* 8(10):e78105.
3. Lipinski KA, Kaniak-Golik A, Golik P (2010) Maintenance and expression of the S. cerevisiae mitochondrial genome: From genetics to evolution and systems biology. *Biochim Biophys Acta* 1797(6-7):1086–1098.
4. Chen XJ, Butow RA (2005) The organization and inheritance of the mitochondrial genome. *Nat Rev Genet* 6(11):815–825.
5. Nunnari J, et al. (1997) Mitochondrial transmission during mating in Saccharomyces cerevisiae is determined by mitochondrial fusion and fission and the intramitochondrial segregation of mitochondrial DNA. *Mol Biol Cell* 8(7):1233–1242.
6. Okamoto K, Perlman PS, Butow RA (1998) The sorting of mitochondrial DNA and mitochondrial proteins in zygotes: Preferential transmission of mitochondrial DNA to the medial bud. *J Cell Biol* 142(3):613–623.
7. Westermann B (2010) Mitochondrial fusion and fission in cell life and death. *Nat Rev Mol Cell Biol* 11(12):872–884.
8. Murley A, et al. (2013) ER-associated mitochondrial division links the distribution of mitochondria and mitochondrial DNA in yeast. *eLife* 2:e00422.
9. Westermann B (2014) Mitochondrial inheritance in yeast. *Biochim Biophys Acta* 1837(7):1039–1046.
10. Bleazard W, et al. (1999) The dynamin-related GTPase Dnm1 regulates mitochondrial fission in yeast. *Nat Cell Biol* 1(5):298–304.
11. Hermann GJ, et al. (1998) Mitochondrial fusion in yeast requires the transmembrane GTPase Fzo1p. *J Cell Biol* 143(2):359–373.
12. Sesaki H, Jensen RE (1999) Division versus fusion: Dnm1p and Fzo1p antagonistically regulate mitochondrial shape. *J Cell Biol* 147(4):699–706.
13. Leibowitz RD (1971) The effect of ethidium bromide on mitochondrial DNA synthesis and mitochondrial DNA structure in HeLa cells. *J Cell Biol* 51(1):116–122.
14. Meeusen S, Nunnari J (2003) Evidence for a two membrane-spanning autonomous mitochondrial DNA replisome. *J Cell Biol* 163(3):503–510.
15. Robinett CC, et al. (1996) In vivo localization of DNA sequences and visualization of large-scale chromatin organization using lac operator/repressor recognition. *J Cell Biol* 135(6 Pt 2):1685–1700.
16. Wang X, Reyes-Lamothe R, Sherratt DJ (2008) Visualizing genetic loci and molecular machines in living bacteria. *Biochem Soc Trans* 36(Pt 4):749–753.
17. Betz JL, Sasmor HM, Buck F, Insley MY, Caruthers MH (1986) Base substitution mutants of the lac operator: In vivo and in vitro affinities for lac repressor. *Gene* 50(1-3):123–132.
18. Miyakawa I, Sando N, Kawano S, Nakamura S, Kuroiwa T (1987) Isolation of morphologically intact mitochondrial nucleoids from the yeast, Saccharomyces cerevisiae. *J Cell Sci* 88(Pt 4):431–439.
19. Jensen RE, Hobbs AE, Cerveny KL, Sesaki H (2000) Yeast mitochondrial dynamics: Fusion, division, segregation, and shape. *Microsc Res Tech* 51(6):573–583.
20. Kowald A, Kirkwood TBL (2011) Evolution of the mitochondrial fusion-fission cycle and its role in aging. *Proc Natl Acad Sci USA* 108(25):10237–10242.
21. Baranowska H, Szcześniak B, Ejchart A, Kruszewskal A, Claisse M (1983) Recombinational analysis of oxi2 mutants and preliminary analysis of their translation products in S. cerevisiae. *Curr Genet* 7(3):225–233.
22. Gruschke S, et al. (2011) Cbp3-Cbp6 interacts with the yeast mitochondrial ribosomal tunnel exit and promotes cytochrome b synthesis and assembly. *J Cell Biol* 193(6):1101–1114.
23. Friedman JR, Nunnari J (2014) Mitochondrial form and function. *Nature* 505(7483):335–343.
24. Shadel GS (1999) Yeast as a model for human mtDNA replication. *Am J Hum Genet* 65(5):1230–1237.
25. Gerhold JM, et al. (2014) Replication intermediates of the linear mitochondrial DNA of Candida parapsilosis suggest a common recombination based mechanism for yeast mitochondria. *J Biol Chem* 289(33):22659–22670.
26. Gerhold JM, Aun A, Sedman T, Jõers P, Sedman J (2010) Strand invasion structures in the inverted repeat of Candida albicans mitochondrial DNA reveal a role for homologous recombination in replication. *Mol Cell* 39(6):851–861.
27. Salje J, Gayathri P, Löwe J (2010) The ParMRC system: Molecular mechanisms of plasmid segregation by actin-like filaments. *Nat Rev Microbiol* 8(10):683–692.
28. Janke C, et al. (2004) A versatile toolbox for PCR-based tagging of yeast genes: New fluorescent proteins, more markers and promoter substitution cassettes. *Yeast* 21(11):947–962.
29. Voth WP, Richards JD, Shaw JM, Stillman DJ (2001) Yeast vectors for integration at the HO locus. *Nucleic Acids Res* 29(12):E59.
30. Thorsness PE, Fox TD (1993) Nuclear mutations in Saccharomyces cerevisiae that affect the escape of DNA from mitochondria to the nucleus. *Genetics* 134(1):21–28.
31. Bonnefoy N, Fox TD (2002) Genetic transformation of Saccharomyces cerevisiae mitochondria. *Methods Enzymol* 350:97–111.
32. Meeusen S, et al. (1999) Mgm101p is a novel component of the mitochondrial nucleoid that binds DNA and is required for the repair of oxidatively damaged mitochondrial DNA. *J Cell Biol* 145(2):291–304.
33. Hoffman CS, Winston F (1987) A ten-minute DNA preparation from yeast efficiently releases autonomous plasmids for transformation of Escherichia coli. *Gene* 57(2-3):267–272.
34. MacAlpine DM, Perlman PS, Butow RA (2000) The numbers of individual mitochondrial DNA molecules and mitochondrial DNA nucleoids in yeast are co-regulated by the general amino acid control pathway. *EMBO J* 19(4):767–775.
35. Carlton PM, et al. (2010) Fast live simultaneous multiwavelength four-dimensional optical microscopy. *Proc Natl Acad Sci USA* 107(37):16016–16022.
36. Meisinger C, Pfanner N, Truscott KN (2006) Isolation of yeast mitochondria. *Methods Mol Biol* 313:33–39.
37. Ameur A, et al. (2011) Ultra-deep sequencing of mouse mitochondrial DNA: Mutational patterns and their origins. *PLoS Genet* 7(3):e1002028.
38. Zeitouni B, et al. (2010) SVDetect: A tool to identify genomic structural variations from paired-end and mate-pair sequencing data. *Bioinformatics* 26(15):1895–1896.
39. Langmead B, Salzberg SL (2012) Fast gapped-read alignment with Bowtie 2. *Nat Methods* 9(4):357–359.
40. Krzywinski M, et al. (2009) Circos: An information aesthetic for comparative genomics. *Genome Res* 19(9):1639–1645.